



Supercritical quasi-conduction states in stochastic Rayleigh–Bénard convection

D. Venturi, M. Choi, G.E. Karniadakis*

Division of Applied Mathematics, Brown University, Providence, RI 02912, USA

ARTICLE INFO

Article history:

Available online 17 April 2012

Keywords:

Natural convection
Uncertainty quantification
Stochastic modeling
High-dimensional systems

ABSTRACT

We study the Rayleigh–Bénard stability problem for a fluid confined within a square enclosure subject to random perturbations in the temperature distribution at both the horizontal walls. These temperature perturbations are assumed to be non-uniform Gaussian random processes satisfying a prescribed correlation function. By using an accurate Monte Carlo method we obtain stochastic bifurcation diagrams for the Nusselt number near the classical onset of convective instability. These diagrams show that random perturbations render the bifurcation process to convection imperfect, in agreement with known results. In particular, the pure conduction state does no longer exist, being replaced by a quasi-conduction regime. We have observed subcritical and *nearly supercritical* quasi-conduction stable states within the range of Rayleigh numbers $Ra = 0$ –4000. This suggests that random perturbations in the temperature distribution at the horizontal walls of the cavity can extend the range of stability of quasi-conduction states beyond the classical bifurcation point $Ra_c = 2585.02$. Analysis of the stochastic bifurcation diagrams shows the presence of a stochastic drift phenomenon in the heat transfer coefficient, especially in the transcritical region. Such stochastic drift is investigated further by means of a sensitivity analysis based on functional ANOVA decomposition.

© 2012 Elsevier Ltd. All rights reserved.

1. Introduction

The classical stability theory of Rayleigh–Bénard convection in an infinite layer of fluid confined between two horizontal isothermal walls with constant but unequal temperatures predicts that the amplitude of the motion undergoes a bifurcation as the Rayleigh number passes through the critical value $Ra_c = 1707.8$ (see, e.g., [1,2]). Such bifurcation characterizes the transition between a pure conduction state and convection. If the flow is laterally confined by rigid and perfectly insulating sidewalls then the critical Rayleigh number usually increases [3–6] due to the *stabilizing effects* of a finite geometry. Furthermore, if there is a small heat transfer through these sidewalls so that the boundary conditions are inconsistent with a state of no motion, then the bifurcation leading to convection is replaced by a *smooth transition* to finite amplitude flow [7]. Such smooth transition has been also predicted theoretically for thermal convection in an infinite fluid layer confined between two rigid horizontal walls with different mean temperatures and *small* spatially periodic perturbations [8].

Considerable research effort has focused on examining the stability of different types of natural convective flows subject to deterministic boundary conditions [9,5,10–12] (see also the interesting recent study [13]). However, not as much work has been done for the case when the boundary conditions are random

processes of *finite amplitude*, although these results would bear upon the importance of ignoring uncertainty when applying classical stability results in real situations, both in laboratory experiments and elsewhere.

Thus, the purpose of the present paper is to examine the effects of temperature perturbations on the classical Rayleigh–Bénard stability problem, namely an unstably stratified fluid contained between two smooth horizontal walls with different mean temperatures. In particular, we will study the prototype problem of a square enclosure having perfectly insulating lateral sidewalls and determine how the random perturbations in the temperature distributions at the horizontal walls affect the stability and the branch points obtained from classical bifurcation analysis. Clearly, when no temperature variations occur along the boundaries convection is possible only when the Rayleigh number is greater than the classical critical value $Ra_c = 2585.02$ [6,5,14]. However, when random temperature variations do occur at the horizontal walls, the bifurcation process leading to convection becomes *imperfect* [15] and the subcritical pure conduction state does no longer exist, being replaced by a *quasi-conduction* regime [8]. This type of flow is characterized by a finite – though perhaps very small – velocity field and it can be observed even at low values of the Rayleigh number.

Many important questions can be addressed in the context of stochastic thermal convection driven by random boundary conditions. For instance: how do the random temperature perturbations affect stability and branch points obtained from classical bifurcation analysis? Is there any connection between the stochastic properties

* Corresponding author.

E-mail address: George_Karniadakis@brown.edu (G.E. Karniadakis).

of the temperature perturbations – such as correlation length and amplitude – and flow stability? Is there a preferential correlation length enhancing the fluid motion and the heat transfer? Is it possible to obtain realizations of stable supercritical quasi-conduction states? In this work we will provide an answer to all these questions by employing a Monte Carlo numerical approach [16,17].

This paper is organized as follows. In Section 2 we formulate the governing equations of the system, i.e., the Oberbeck–Boussinesq approximation to convection via the vorticity transport equation [18,19]. In Section 3 we characterize the random temperature perturbations at the horizontal walls of the cavity in terms of Karhunen–Loève expansions satisfying a prescribed Gaussian correlation function. In Section 4 we investigate the effects of these perturbations – parametrized in terms of their correlation length and amplitude – on the onset of convective instability and we determine useful stochastic bifurcation diagrams for the Nusselt number near the onset. The existence of supercritical quasi-conduction states is discussed in Section 5. By using the ANOVA method [20–23], in Section 6 we study the sensitivity of the integrated Nusselt number with respect to variations in the amplitude of different harmonics appearing in the random boundary conditions. This allows us to identify the most effective spatial frequency in the temperature distributions at the horizontal walls enhancing the heat transfer coefficient. Finally, the main findings and their implications are summarized in Section 7. We also include two brief appendices dealing with the Galerkin discretization of the Oberbeck–Boussinesq equations and the description of the ANOVA technique for sensitivity analysis, respectively.

2. Governing equations

Let us consider the Rayleigh–Bénard stability problem for a fluid confined within a square enclosure heated from below and cooled from above and subject to random perturbations in the temperature distribution at both the horizontal walls. The lateral sidewalls are assumed to be perfectly insulating (see Fig. 1). We assume that the flow can be described in terms the dimensionless Oberbeck–Boussinesq approximation written as a vorticity transport equation in streamfunction-only formulation

$$-\frac{\partial \psi}{\partial y} \frac{\partial (\nabla^2 \psi)}{\partial x} + \frac{\partial \psi}{\partial x} \frac{\partial (\nabla^2 \psi)}{\partial y} = -Pr \nabla^4 \psi + RaPr \frac{\partial T}{\partial x}, \tag{1}$$

$$\frac{\partial \psi}{\partial y} \frac{\partial T}{\partial x} - \frac{\partial \psi}{\partial x} \frac{\partial T}{\partial y} = \nabla^2 T. \tag{2}$$

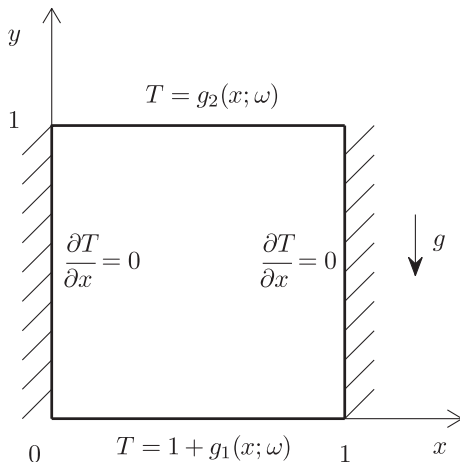


Fig. 1. Schematic of the dimensionless geometry and dimensionless temperature boundary conditions. The random perturbations g_1 and g_2 are assumed to be zero mean Gaussian processes. The velocity boundary conditions are of no-slip type, i.e., $\psi = \partial\psi/\partial x = \partial\psi/\partial y = 0$ at the solid walls.

This system is supplemented with the boundary conditions

$$\psi = 0, \quad \frac{\partial \psi}{\partial x} = 0, \quad \frac{\partial \psi}{\partial y} = 0, \tag{3}$$

along all the sidewalls of the cavity as well as

$$T = 1 + g_1(x; \omega), \quad y = 0, \quad 0 \leq x \leq 1, \tag{4}$$

$$T = g_2(x; \omega), \quad y = 1, \quad 0 \leq x \leq 1, \tag{5}$$

$$\frac{\partial T}{\partial x} = 0, \quad x = 0, \quad 0 \leq y \leq 1, \tag{6}$$

$$\frac{\partial T}{\partial x} = 0, \quad x = 1, \quad 0 \leq y \leq 1. \tag{7}$$

In the equations above $\psi(x,y;\omega)$ and $T(x,y;\omega)$ denote the random streamfunction and temperature fields while Ra and Pr are the Rayleigh and the Prandtl numbers, respectively. The variable ω appearing in $\psi(x,y;\omega)$ and $T(x,y;\omega)$ identifies a possible outcome of the streamfunction and the temperature for a specific realization of the random temperature perturbations $g_1(x,\omega)$ and $g_2(x,\omega)$ at the horizontal walls. A rigorous mathematical definition of these perturbations will be given in the subsequent section.

All quantities in Eqs. (1)–(7) have been made dimensionless by scaling lengths with the side length of the cavity L , streamfunction with the kinematic viscosity ν , time with L^2/ν and temperature with a reference temperature difference $\Delta\theta_r$ which is defined to be the difference between the averages of the two temperature processes at the horizontal walls.¹ With this rescaling, the Rayleigh and the Prandtl numbers are obtained as

$$Ra = \frac{g\beta L^3 \Delta\theta_r}{\alpha\nu}, \quad Pr = \frac{\nu}{\alpha}, \tag{8}$$

where g , β and α are the acceleration of gravity, the isobaric compressibility coefficient and the thermal diffusivity of the fluid, respectively. We notice, that this type of adimensionalization is not effective when the average temperature is the same along the two horizontal walls. In fact, in this case the reference temperature difference $\Delta\theta_r$ becomes 0 but we still could have convection due to temperature variations at the boundaries. This case will not be considered in the present study. At this point, it is convenient to transform the non-homogeneous temperature boundary conditions into homogeneous ones. This is achieved by defining the new field

$$T^*(x,y;\omega) \stackrel{\text{def}}{=} T(x,y;\omega) + (y-1)(g_1(x;\omega) + 1) - yg_2(x;\omega), \tag{9}$$

where $g_1(x;\omega)$ and $g_2(x;\omega)$ are random processes satisfying adiabatic boundary conditions at $x = 0$ and $x = 1$, i.e.,

$$\left. \frac{\partial g_i}{\partial x} \right|_{x=0,1} = 0, \quad \text{for } i = 1, 2. \tag{10}$$

Eq. (9) can be inverted as

$$T = T^* + (1-y)(g_1 + 1) + yg_2. \tag{11}$$

From Eq. (11) we obtain

$$\frac{\partial T}{\partial x} = \frac{\partial T^*}{\partial x} + y \left(\frac{\partial g_2}{\partial x} - \frac{\partial g_1}{\partial x} \right) + \frac{\partial g_1}{\partial x}, \tag{12}$$

$$\frac{\partial T}{\partial y} = \frac{\partial T^*}{\partial y} + (g_2 - g_1) - 1, \tag{13}$$

$$\nabla^2 T = \nabla^2 T^* + y \left(\frac{\partial^2 g_2}{\partial x^2} - \frac{\partial^2 g_1}{\partial x^2} \right) + \frac{\partial^2 g_1}{\partial x^2}. \tag{14}$$

Finally, a substitution of Eqs. (12)–(14) into Eqs. (1) and (2), respectively, yields the system

¹ The dimensionless temperature field is defined as $T = (\theta - \theta_c)/\Delta\theta_r$ where θ_c denotes the average of random temperature distribution at the upper horizontal wall.

$$-\frac{\partial\psi}{\partial y}\frac{\partial(\nabla^2\psi)}{\partial x} + \frac{\partial\psi}{\partial x}\frac{\partial(\nabla^2\psi)}{\partial y} = -Pr\nabla^4\psi + RaPr\left(\frac{\partial T^*}{\partial x} + y\left(\frac{\partial g_2}{\partial x} - \frac{\partial g_1}{\partial x}\right) + \frac{\partial g_1}{\partial x}\right), \tag{15}$$

$$\frac{\partial\psi}{\partial y}\left(\frac{\partial T^*}{\partial x} + y\left(\frac{\partial g_2}{\partial x} - \frac{\partial g_1}{\partial x}\right) + \frac{\partial g_1}{\partial x}\right) = \nabla^2 T^* + \frac{\partial^2 g_1}{\partial x^2}\frac{\partial\psi}{\partial x}\left(\frac{\partial T^*}{\partial x} + (g_2 - g_1) - 1\right) + y\left(\frac{\partial^2 g_2}{\partial x^2} - \frac{\partial^2 g_1}{\partial x^2}\right). \tag{16}$$

The boundary conditions associated with Eqs. (15) and (16) are now homogeneous. In Appendix A we obtain the Galerkin discretization of this system in terms of eigenfunctions of proper eigenvalue problems.

3. Characterization of temperature perturbations at the horizontal walls

We shall assume that the temperature perturbations $g_1(x; \omega)$ and $g_2(x; \omega)$ are zero mean random processes satisfying adiabatic boundary conditions at $x = 0$ and $x = 1$. In order to represent these processes, let us first consider a suitable orthonormal basis obtained from the classical Sturm–Liouville eigenvalue problem [24,25]

$$\frac{d^2\phi}{dx^2} + a^2\phi = 0, \quad \text{with} \quad \frac{d\phi(0)}{dx} = \frac{d\phi(1)}{dx} = 0. \tag{17}$$

The normalized eigenfunctions solving (17) are

$$\phi_0(x) = 1, \quad \phi_n(x) = \sqrt{2} \cos(n\pi x) \quad n = 1, 2, 3, \dots \tag{18}$$

Thus, if $h(x; \omega)$ is a zero-mean process satisfying adiabatic boundary conditions at $x = 0$ and $x = 1$, then we have the following spectral representation² [26]

$$h(x; \omega) = \sigma \sum_{k=1}^{\infty} a_k(\omega) \phi_k(x), \tag{19}$$

where σ is a real parameter that characterizes the amplitude of the process while

$$a_k(\omega) = \frac{1}{\sigma} \int_0^1 h(x; \omega) \phi_k(x) dx \tag{20}$$

are pairwise uncorrelated random variables. The covariance of the process $h(x; \omega)$ has the obvious representation

$$C(x, x') \stackrel{\text{def}}{=} \frac{\langle h(x; \omega)h(x'; \omega) \rangle}{\sigma^2} = \sum_{n=1}^{\infty} \langle a_n^2 \rangle \phi_n(x)\phi_n(x'), \tag{21}$$

where $\langle \cdot \rangle$ denotes the average with respect to the joint probability measure of the variables $\{a_k(\omega)\}$. An important question at this point is: if we arbitrarily prescribe a covariance function, say $C^*(x, y)$, can we determine a set of uncorrelated random variables $a_k^*(\omega)$ such that (21) is satisfied? The answer is obviously affirmative, provided the prescribed covariance satisfies the boundary conditions

$$\frac{\partial C^*(x, y)}{\partial x} \Big|_{x=0} = 0 \quad \text{and} \quad \frac{\partial C^*(x, y)}{\partial x} \Big|_{x=1} = 0, \quad \forall y \in [0, 1], \tag{22}$$

as well as the zero-mean constraint

$$\int_0^1 C^*(x, y) dx = 0, \quad \forall y \in [0, 1]. \tag{23}$$

² Note that all the basis functions $\phi_k(x)$ (except ϕ_0) integrate to zero and satisfy adiabatic boundary conditions at $x = 0$ and $x = 1$.

If $C^*(x, y)$ does not satisfy such conditions then it is possible to enforce them through projection. To this end, let us first consider the (positive) Fourier coefficients

$$\langle b_n^2 \rangle \stackrel{\text{def}}{=} \int_0^1 \int_0^1 C^*(x, x') \phi_n(x) \phi_n(x') dx dx', \quad n \geq 1, \tag{24}$$

obtained by projecting the arbitrarily prescribed kernel $C^*(x, x')$ onto the basis $\{\phi_k\}$. This operation basically removes every spatial gradient at the boundaries $x = 0$ and $x = 1$ and it makes the assigned correlation zero spatial mean, in the sense of (23). Next, let us consider the spectral expansion of the kernel $C^*(x, x')$ in terms of its (positive) eigenvalues λ_k and eigenfunctions ψ_k

$$C^*(x, x') = \sum_{k=1}^{\infty} \lambda_k \psi_k(x) \psi_k(x'). \tag{25}$$

A substitution this expression into (24) immediately yields

$$\langle b_n^2 \rangle = \sum_{k=1}^{\infty} \lambda_k \left[\int_0^1 \psi_k(x) \phi_n(x) dx \right]^2, \quad n \geq 1. \tag{26}$$

At this point it is easy to check that if $\{\xi_k(\omega)\}$ is any set of zero-mean and uncorrelated random variables with unit variance (i.e., $\langle \xi_k^2 \rangle = 1$) then the process

$$h(x; \omega) = \sigma \sum_{k=1}^{\infty} \langle b_k^2 \rangle^{1/2} \xi_k(\omega) \phi_k(x) \tag{27}$$

satisfies the adiabatic boundary conditions at $x = 0$ and $x = 1$ as well as the zero spatial mean constraint and it has the following covariance

$$\tilde{C}^*(x, x') = \sum_{n=1}^{\infty} \langle b_n^2 \rangle \phi_n(x) \phi_n(x'). \tag{28}$$

The technique just discussed can be considered as particular case of the *spectral transformation method* [27,28] where an assigned correlation kernel is generated by assigning the spectrum relatively to a specified orthogonal basis. In this paper we will employ the following Gaussian covariance (see [29])

$$C^*(x, x') = \exp \left[-6 \frac{(x - x')^2}{l_c^2} \right]. \tag{29}$$

This allows us to represent the temperature perturbations g_1 and g_2 as the following Karhunen–Loève expansions

$$g_i(x; \omega) = \sigma \sum_{k=1}^M \langle b_k^2 \rangle^{1/2} \xi_k^{(i)}(\omega) \phi_k(x), \quad i = 1, 2, \tag{30}$$

where $\xi_k^{(i)}$ ($i = 1, 2; k = 1, 2, \dots, M$) are zero-mean uncorrelated Gaussian random variables with unit variance. Several samples of the processes (30) are shown in Fig. 2(b) for different correlation lengths l_c and perturbation amplitude σ set at 5% of the reference temperature difference between the horizontal walls. Physically, this means a temperature perturbation with amplitude 1 K for temperature differences of about 20 K. We remark that the truncation process in the series expansion (30) has to be performed with some care, in such a way that the energy of the neglected modes is actually negligible. To this end, we examine the relative energy of the temperature perturbations

$$e_f(M) \stackrel{\text{def}}{=} \frac{E_f(M)}{E_f(\infty)}, \quad \text{where} \quad E_f(M) \stackrel{\text{def}}{=} \sum_{n=1}^M \langle b_n^2 \rangle \tag{31}$$

and choose the total number of terms M in such a way that e_f is greater than a specified *cutoff value*. In Fig. 2(a) we show the plots of $e_f(M)$ corresponding to different dimensionless correlation lengths while in Table 1 we report on the dimensionality M – i.e., the total number of terms – of the spectral representation (30) for

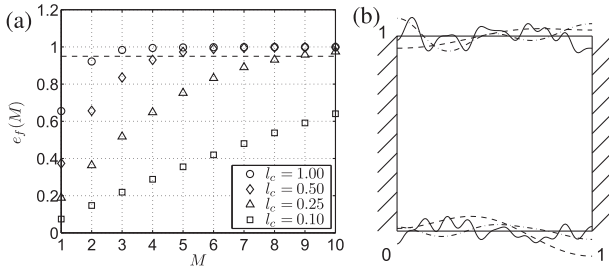


Fig. 2. (a) Relative energy of a truncated Karhunen–Loève expansion of the temperature processes at the horizontal walls as a function of the number of terms retained in the representation for different correlation lengths (all symbols are defined in Eqs. (29)–(31)). We also show the relative energy cutoff set at 95% (dashed line). (b) Samples of temperature perturbations at lower and upper horizontal walls for correlation lengths $l_c = 1$ (—), $l_c = 0.5$ (---) and $l_c = 0.1$ (· · ·). The perturbation amplitude σ here is set at 5% of the reference temperature difference.

Table 1
Effects of correlation length l_c on the dimensionality M of the temperature representation at each horizontal boundary. The energy cutoff is set at 95% of the total energy of the process.

l_c	∞	2	1	0.5	0.25	0.1	0.05	0.025	0.01
M	1	2	3	5	9	22	44	87	199

a 95% cutoff threshold. We notice that as the correlation length goes to zero the temperature perturbation at the horizontal walls approaches an independent increment process [30]. Even for temperature perturbations having correlation length l_c about 0.1 (scaled on the side length of the cavity) the number of expansion terms M becomes relatively large. Specifically, since we have two random boundaries, the case $l_c = 0.1$ results in a stochastic system forced by 44 (22 + 22) random variables (see Table 1). The simulation of these high-dimensional systems requires appropriate numerical techniques [23,31–37] (see also [38]). In this work we will employ a Monte Carlo method but also polynomial chaos with adaptive ANOVA can be used [22].

In the following sections, unless explicitly stated, the perturbation amplitude σ of the temperature processes (30) is set at 5% of the reference temperature difference.

4. Stochastic bifurcations and stability of steady state convection

In previous work [6] we have obtained bifurcation diagrams for natural convective flows within square cavities subject to uniform temperature boundary conditions. We have observed the coexistence of multiple stable steady states, in agreement with recent results [12,11,10,9], for fixed values of Rayleigh and Prandtl numbers. The time-asymptotic steady state was found to be dependent on the initial flow condition. In the presence of random temperature perturbations at the horizontal walls of the cavity, multiple stable states can still coexist, but the mechanism of their formation is substantially different from the uniform boundary condition case. Indeed, as we can see from Eqs. (15) and (16), the random perturbations g_1 and g_2 break the symmetry of the system, i.e., the steady-state convection pattern do not satisfy, in general, the discrete symmetry group described in [6]. Therefore, the symmetry-induced multiplicity of supercritical states in this case is replaced by a more physical ensemble of flows in a one-to-one correspondence with specific boundary and initial conditions.³

³ We remark that for very specific realizations of the temperature processes at the horizontal walls, convection can still satisfy the discrete symmetry group described in [6]. However, from a statistical viewpoint the probability that this happens is actually zero.

We have identified many different steady-state stable convection patterns and corresponding temperature fields. These include *subcritical* and *supercritical* quasi-conduction states for which the kinetic energy of the flow turns out to be very small. In Fig. 3 we show typical temperature fields and flow patterns corresponding to specific realizations of the temperature boundary conditions.

4.1. Bifurcation diagrams for the Nusselt number

As is well known, a sudden change in the slope the Nusselt number versus the Rayleigh number usually identifies a transition between different flow states. In the particular case of *uniform* temperature boundary conditions the first one of these transitions characterizes the onset of convective instability [12,5] and, for the geometry shown in Fig. 1, it can be clearly identified at $Ra_c = 2585.02$. However, in the presence of random temperature perturbations along the horizontal walls of the cavity, the precise determination of the critical Rayleigh number can be rather difficult. In fact, as pointed out by Ahlers et al. in [15], such perturbations render the bifurcation process to convection *imperfect* and, strictly speaking, a critical Rayleigh number does not even exist in the usual sense since convection occurs for *all* values of Ra . However, as the Rayleigh number approaches the classical critical value, the amplitude of convection increases greatly, and therefore it still makes sense to define a “critical” regime near the classical onset.

In Fig. 4 we show the bifurcation diagrams for the integrated Nusselt number

$$Nu(\omega) \stackrel{\text{def}}{=} \int_0^1 \frac{\partial T(x, y; \omega)}{\partial y} \Big|_{y=0} dx, \tag{32}$$

versus the Rayleigh number. These diagrams are obtained by first sampling the temperature distribution at the horizontal walls for different perturbation amplitudes and correlation lengths and then compute the corresponding *stable*⁴ convective flow through the Galerkin method outlined in Appendix A. Thus, most of the bifurcation diagrams shown in this section are not obtained through continuation but rather through random sampling. The main reason why we decided to follow this approach is that in this way we do not need to perform continuation for each specific realization of the random boundary conditions. Given the fact that we consider an ensemble of 10^5 realizations for each correlation length and perturbation amplitude, it is easy to understand that a standard continuation approach would not be viable in practice. In the plots of Fig. 4 we also include the classical bifurcation diagram for *deterministic* uniform boundary conditions (dashed lines). This case has been obtained by using continuation techniques [6]. Specifically, the continuation algorithm employed to track steady states uses a prediction-correction scheme based on the Moore–Penrose matrix pseudoinverse. Mathematical details may be found in [39] (see also [40]).

Note that the bifurcation diagrams obtained for temperature perturbations with correlation lengths $l_c = 1$ and $l_c = 0.5$ are very similar. This can be explained by noting that the temperature perturbations at the horizontal walls of the cavity are quite similar to each other in these cases (see Fig. 2(b)). Among many possible convection patterns, our numerical results show that it is possible to obtain realizations of *nearly supercritical* (stable) quasi-conduction states. In other words, it seems that random perturbations can stabilize the quasi-conduction state beyond the classical bifurcation point. This rather surprising result will be discussed further in the next section.

⁴ We report only on *stable* steady states. Other *unstable* states are present as well, but these are not shown in Fig. 4.

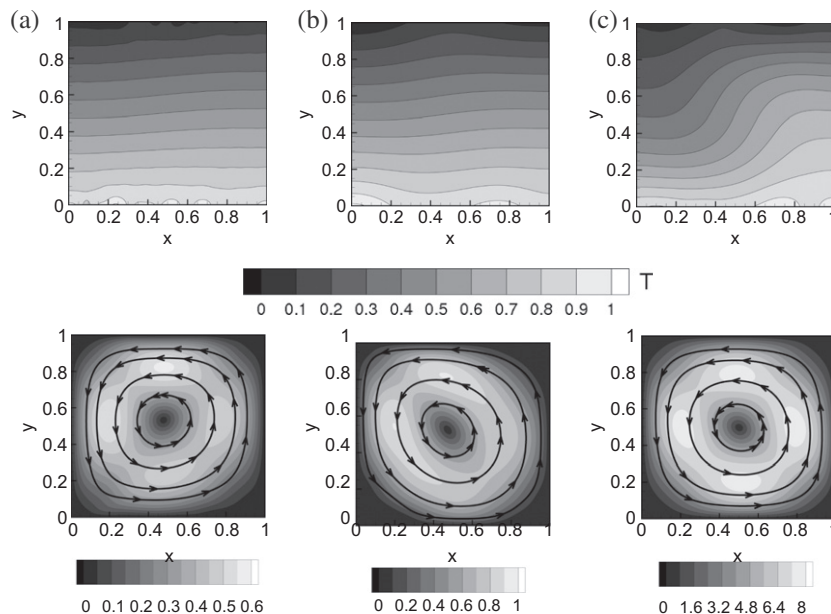


Fig. 3. Typical temperature fields (top row) and streamlines of the velocity field superimposed to the modulus of velocity (lower row) for specific realizations of the temperature distribution at the horizontal walls of the cavity. The correlation length of the temperature perturbations at the horizontal walls is set to $l_c = 0.1$ (a), $l_c = 0.5$ (b) $l_c = 0.25$ (c). Show are: (a) a *subcritical* quasi-conduction state at $Ra = 1946$, (b) a *supercritical* quasi-conduction state $Ra = 2650$ and (c) a fully developed one-roll convection pattern at $Ra = 3500$.

4.2. Statistical analysis of the heat transfer

In Fig. 5(a) we plot the probability density function of the integrated Nusselt number at Rayleigh number 3000 and Prandtl number 0.7 for boundary perturbations with different correlation lengths. Each probability density is estimated by using a *non-parametric* kernel regression method based on the available temperature samples. Specifically, we have computed 10^5 flow samples for each selected Rayleigh number, correlation length and amplitude of the temperature perturbations at the horizontal walls.

As it is seen from Fig. 5(a), these random perturbations can increase or decrease the global heat transfer relatively to the uniform case. In the mean sense, however, it turns out that the heat transfer is enhanced, especially in the transcritical region (see Fig. 6). Similarly, in Fig. 5(b), we plot the probability density functions of the integrated Nusselt number at different Rayleigh numbers for boundary perturbations with correlation length $l_c = 0.5$. We notice that at $Ra = 1000$ the probability density of Nu is rather peaked around $Nu = 1$, suggesting a high probability of quasi-conduction regime. In the transcritical region we also observe a variation of the probability density function that becomes *approximately Gaussian* when convection is fully developed. Note also that for supercritical flows, the probability density of the integrated Nusselt number is *continuously supported*. This suggests that for the correlation lengths and the perturbation amplitudes considered in this paper it seems that there exist only one possible supercritical convection pattern, i.e., a one-roll flow. In other words, the ensemble of stable flows is continuous and composed by one-roll patterns, with the exception of some subcritical quasi-conduction states.

Next, we determine the average and the range of the integrated Nusselt number as a function of the Rayleigh number for different correlation lengths. This study helps us in clarifying if the correlation length of the temperature perturbations at the horizontal walls has an influence on the averaged heat transfer within the cavity. The results of our computations are shown in Fig. 6(a). As easily seen, random temperature perturbations induce a *stochastic drift* in the transcritical region yielding to an increment of the average heat transfer. This increment depends on the correlation length

of the temperature processes, i.e., there are preferential values of temperature correlation lengths that trigger convection patterns that are more effective for what concerns the heat transfer. Note, however, that the heat transfer enhancement is rather weak in all cases we have considered, quantifiable in approximately 10% within the transcritical region. Also, when convection is fully developed the stochastic drift disappears and the probability density of the integrated Nusselt number becomes very similar to a Gaussian distribution (see Fig. 5(b)).

It is interesting to study the relation between the integrated Nusselt number and the dimensionless kinetic energy of the fluid in more detail. Our first finding is that the correlation coefficient between these two quantities is approximately one in all cases we have considered in this paper. This suggests that there exist a linear relation between the Nusselt number and dimensionless kinetic energy of the fluid at Prandtl number 0.7. This relation is shown in Fig. 6(b) where we plot the integrated Nusselt number versus the kinetic energy of the fluid for different Rayleigh numbers. The existence of a linear relation between the integrated Nusselt number and the dimensionless kinetic energy implies that heat transfer is primarily determined by advection, even in the quasi-conduction regime.

5. Subcritical and supercritical quasi-conduction states

The existence of subcritical quasi-conduction states has been theoretically predicted by Kelly and Pal in [8] for an infinite layer of fluid with small periodic temperature variations at the horizontal walls. By means of perturbation analysis, they have found that convection can occur even for Rayleigh numbers less than the critical one ($Ra_c = 1707.8$ for the infinite layer). The corresponding Nusselt number was found to be a function of the Rayleigh number, the Prandtl number and the modulation amplitude. The perturbation approach of Kelly and Pal, however, cannot be easily extended to the present flow problem because of the random boundary conditions. In fact, these processes could depend on many random variables (see Table 1) and therefore it is not easy to select a

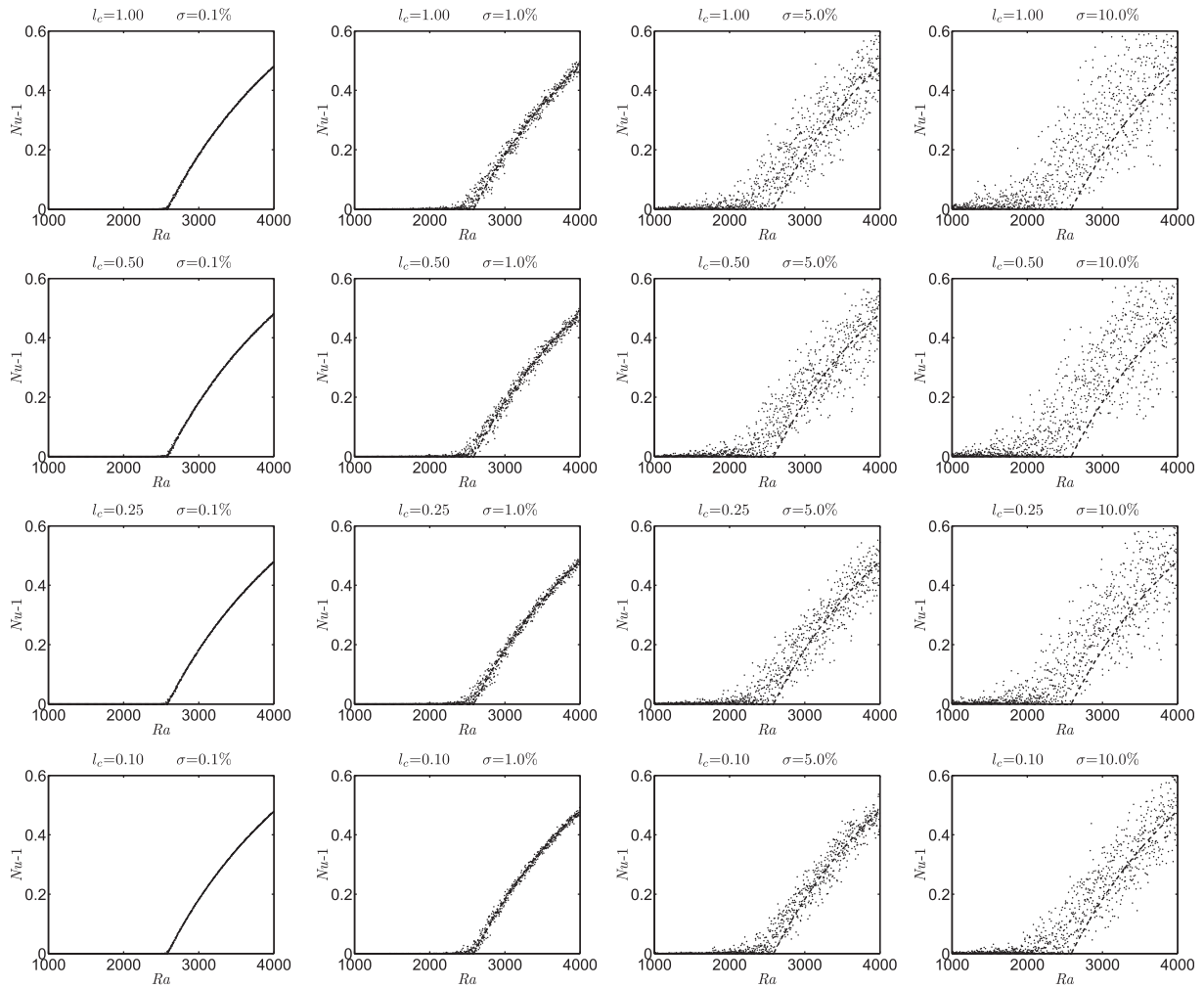


Fig. 4. Bifurcation diagrams near the onset of convective instability for random perturbations in the temperature distribution at the horizontal walls of the cavity. Shown are samples of the integrated Nusselt number versus the Rayleigh number corresponding to different choices of the correlation length (l_c) and the perturbation amplitude (σ) of the temperature boundary processes. The dashed line in each plot represents the classical bifurcation diagram obtained for deterministic, spatially uniform, temperature conditions. The critical Rayleigh number, in this case, is $Ra_c = 2585.02$ (see [6,5]).

significant perturbation parameter quantifying the “amplitude of convection”.⁵ A criterion to identify a quasi-conduction state may be based on the analysis of the dimensionless temperature field within the cavity. In particular, a comparison between the pure conduction solution and the convection solution can reveal if there is a significant temperature transport associated with the fluid motion. We recall that the steady-state pure conduction solution can be obtained by integrating the Poisson’s equation

$$\nabla^2 T^* = -y \left(\frac{\partial^2 g_2}{\partial x^2} - \frac{\partial^2 g_1}{\partial x^2} \right) - \frac{\partial^2 g_1}{\partial x^2} \quad (33)$$

for homogeneous boundary conditions ($T^* = 0$ at the horizontal walls and $\partial T^*/\partial x = 0$ at the sidewalls of the cavity), and then using Eq. (11).

A simpler criterion to identify a quasi-conduction regime is based on the integrated Nusselt number itself. In practice, we

can define a threshold for Nu below which we can state that convection is neglectable. At Prandtl number 0.7, this is equivalent to selecting a threshold for the dimensionless kinetic energy of the fluid. In fact, as we have pointed out in the previous section, the integrated Nusselt number and the dimensionless kinetic energy of the fluid are extremely well correlated in all cases we have considered in this paper. The selection of a threshold value for the integrated Nusselt number obviously introduces some arbitrariness in the definition of quasi-conduction states. This arbitrariness, however, is of the same type as that of defining a critical Rayleigh number in presence of random boundary conditions.

Given these remarks, let us set the threshold $Nu_{tr} = 1.02$ for quasi-conduction states. This choice is based on the analysis of many different realizations of subcritical flows where the temperature field is not significantly transported by the velocity field. In these conditions we have found the Nusselt number rarely exceeds the value 1.02. The selected threshold $Nu_{tr} = 1.02$ discriminates among those flows whose heat transfer differs at most by 2% with respect to pure conduction. In Fig. 7 we sketch the graphical procedure for the identification of quasi conduction-states according to the proposed criterion. An analysis of the stochastic flow field near the onset of convection reveals that random temperature perturbations at the horizontal boundaries can stabilize a *nearly supercritical* quasi-conduction regime. This region is indicated in Fig. 7(b) for

⁵ From a theoretical viewpoint, a supercritical stable state might be investigated by analyzing the Oberbeck–Boussinesq system, in any representation. In particular, one can consider the Galerkin discretization obtained in Appendix A, expand the solution near $a_k \equiv 0$ and $b_k \equiv 0$ and try to determine whether there exist a set of coefficients for which the real part of the largest Jacobian eigenvalue is negative. This leads to a complex relation between the forcing (buoyancy) term in the Navier–Stokes equation and the Rayleigh number.

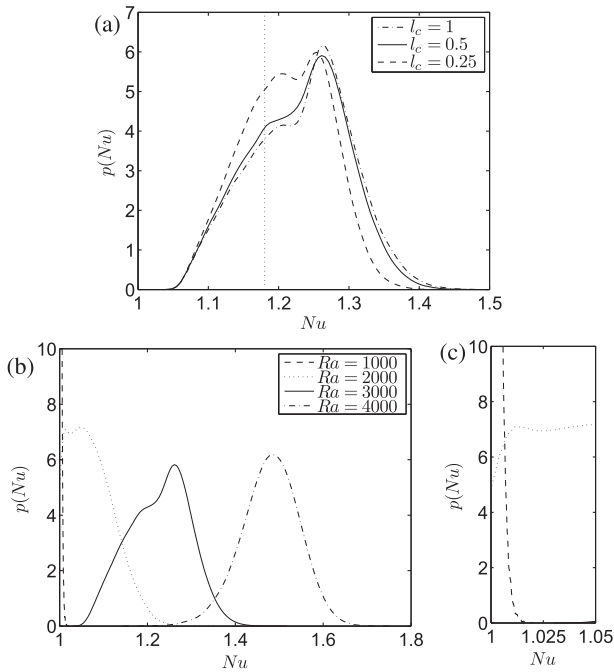


Fig. 5. (a) Probability density functions of the integrated Nusselt number at Rayleigh number $Ra = 3000$ for boundary perturbations of different correlation lengths. The vertical line indicates the deterministic Nusselt number at $Ra = 3000$ corresponding to uniform boundary conditions. (b) Probability density functions of the integrated Nusselt number at different Rayleigh numbers for $l_c = 0.5$: $Ra = 1000$ (---), $Ra = 2500$ (···), $Ra = 3000$ (-) and $Ra = 4000$ (- - -). Figure (c) is a zoom-in of figure (b).

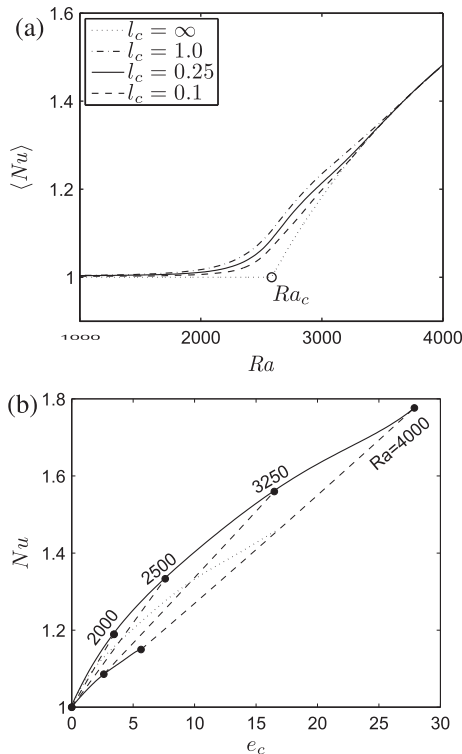


Fig. 6. (a) Mean of the integrated Nusselt number versus the Rayleigh number for boundary perturbations of different correlation lengths. (b) Integrated Nusselt number versus the dimensionless kinetic energy (e_c) of the fluid at Prandtl number 0.7. The correlation length of the temperature perturbations is set to $l_c = 1$. We show the mean (···) and the min–max band (-), which is parametrized with the Rayleigh number Ra . The curves at constant Ra (- -) are simple straight lines due to the very high correlation coefficient between Nu and e_c at Prandtl number 0.7.

boundary perturbations having correlation length $l_c = 0.5$. Thus, random perturbations can extend the domain of stability of quasi-conduction states beyond the classical bifurcation point. In Fig. 3(b) we show one of these states at Rayleigh number 2650. An important question at this point is: *What is the probability that a supercritical stable quasi-conduction state develops within the cavity?*

In order to answer this question, in Fig. 8 we plot the probability of occurrence of quasi-conduction states within the whole range of Rayleigh numbers considered in this paper, for boundary perturbations of different correlation lengths. This probability function is estimated by counting the relative number of quasi-conduction states, i.e., the states whose energy is within the quasi-conduction energy band. As easily seen, the probability curve is monotonic and it reaches the value zero (impossible event) approximately at $Ra \approx 2800$ in all cases. We also notice that the occurrence of a nearly supercritical quasi-conduction state is rather unlikely (see Fig. 8(b)) and it weakly depends on the correlation length of the temperature perturbations at the horizontal walls. In particular, smaller correlation lengths yield higher probabilities of supercritical quasi-conduction states. Clearly, all these results depend on the choice of the quasi-conduction energy band. In other words, a different selection of the threshold for the integrated Nusselt number or the kinetic energy of the fluid could yield quantitatively different but qualitatively similar conclusions. In particular, if we increase the threshold level for the Nusselt number above 1.02 we obtain a translation to the right of all the curves plotted in Fig. 8.

6. Sensitivity analysis

In this section we employ the functional ANOVA technique [23,20,41,42,33] (see also Appendix B) in order to identify which harmonic in the Fourier series representation of the random

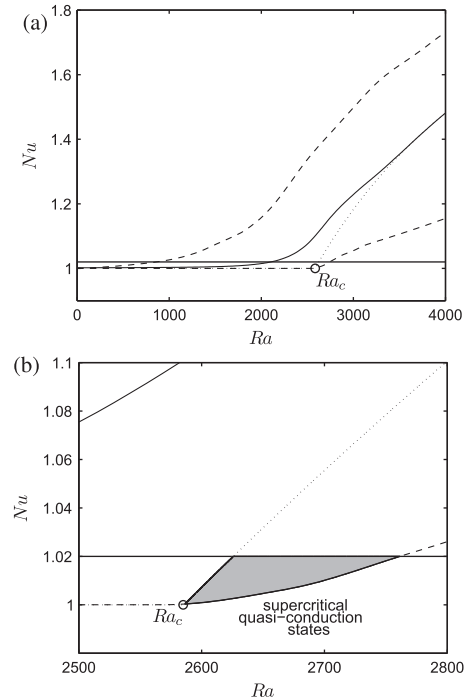


Fig. 7. Threshold criterion for the identification of quasi-conduction states. These diagrams refer to the case where the boundary perturbations have correlation length $l_c = 0.5$. We show the mean Nusselt number (-), the minimum and the maximum Nusselt numbers (- -) and the classical bifurcation diagram (···) obtained for spatially-uniform deterministic boundary conditions. Figure (b) is a zoom-in of figure (a).

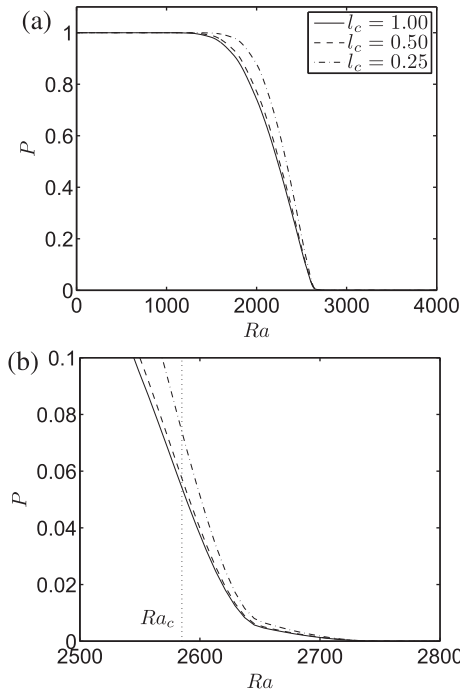


Fig. 8. Probability that a stable quasi-conduction state develops within the cavity as a function of the Rayleigh number and the correlation length of the temperature processes at the horizontal walls of the cavity. Figure (b) is a zoom-in of figure (a).

temperature boundary conditions is responsible the heat transfer enhancement and also triggers the transition from quasi-conduction to fully developed convection. This sensitivity study allows us to make inferences about the most important unstable modes and, in some sense, it is similar to the perturbation approach adopted by Kelly and Pal [8] for the infinite fluid layer.

Thus, let us consider an ANOVA expansion of the Nusselt number in terms of the set of random variables representing the *amplitude* of the boundary conditions

$$Nu(\zeta) = Nu_0 + \sum_{i=1}^{2M} Nu_i(\zeta_i) + \sum_{i<j}^{2M} Nu_{ij}(\zeta_i, \zeta_j) + \sum_{i<j<k}^{2M} Nu_{ijk}(\zeta_i, \zeta_j, \zeta_k) + \dots, \tag{34}$$

where

$$\zeta \stackrel{\text{def}}{=} [\zeta_1^{(1)}, \dots, \zeta_M^{(1)}, \zeta_1^{(2)}, \dots, \zeta_M^{(2)}]. \tag{35}$$

We recall that M depends on the spatial correlation length of the temperature process. Specifically, for $l_c = 0.5$ – which is the case we examine here – we obtain a total number of 10 (5 + 5) random variables. In other words, the *nominal dimension* [33] of the parameter space here is 10 (see Table 1).

The sensitivity (in the sense of Sobol [43]) of the integrated Nusselt number with respect to the amplitude of the boundary modes can be studied as a function of the Rayleigh number. This provides an insight, e.g., on which harmonic of the temperature distribution at the boundaries (first-order interaction) or combination of harmonics (higher-order interactions) are most important in the transition from quasi-conduction to fully developed convection. The results of this study are summarized in Fig. 9 where we plot the averaged global sensitivity factors for first-, second- and third-order interaction terms corresponding to all five parameters $[\zeta_1^{(1)}, \dots, \zeta_5^{(1)}]$ defining the random temperature process at the lower horizontal wall. These sensitivity factors are explicitly defined as

$$Z_i^{(1)} \stackrel{\text{def}}{=} \frac{\sigma^2[Nu_i]}{\sigma^2[Nu]}, \tag{36}$$

$$Z_i^{(2)} \stackrel{\text{def}}{=} \sum_j \frac{\sigma^2[Nu_{ij}]}{\sigma^2[Nu]}, \tag{37}$$

$$Z_i^{(3)} \stackrel{\text{def}}{=} \sum_{j,k} \frac{\sigma^2[Nu_{ijk}]}{\sigma^2[Nu]}, \tag{38}$$

where Nu_i , Nu_{ij} and Nu_{ijk} are the interaction terms in Eq. (34) while $\sigma^2[\cdot]$ denotes the variance operator (see Appendix B for further details).

As seen from the plots of $Z_i^{(k)}$ ($k=1,2,3$), the subcritical quasi-conduction region ($Ra < Ra_c$) is rather sensitive to variations in the amplitude of all the temperature boundary modes. We also notice that the highest sensitivity of the Nusselt number within the transcritical region $Ra \simeq 2700 - 3000$ is achieved by the variable number “1” (see the plots of $Z_1^{(j)}$). This variable characterizes the amplitude of the lowest frequency mode in the Fourier expansion of the temperature boundary conditions, i.e., $\cos(\pi x)$. Therefore, the heat transfer enhancement in the transcritical region, i.e., the

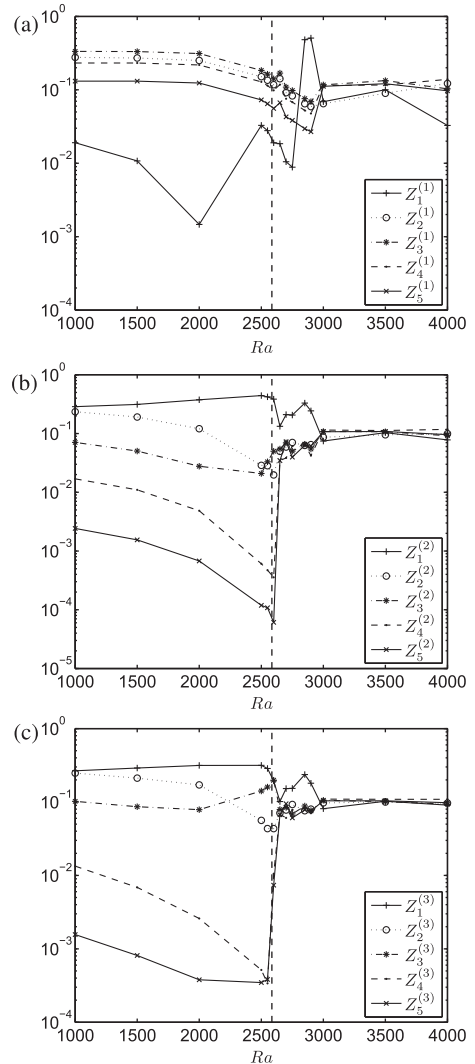


Fig. 9. Averaged global sensitivity indices of different terms in the ANOVA decomposition of the Nusselt number for variations in the amplitude of the harmonics representing the temperature boundary condition at the lower horizontal wall. Shown are sensitivities of (a) first-order, (b) second-order and (c) third-order interaction terms versus the Rayleigh number. The vertical dashed line in each plot identifies the classical bifurcation point at $Ra_c = 2585$.

stochastic drift phenomenon described in Section 4.2, is mainly influenced by such harmonic.

The transition from quasi-conduction to fully developed convection is captured by the second- and the third-order interaction terms. In fact, as seen from Fig. 9(b) and (c), the global sensitivity factors of second- and third-order interactions undergo a sudden jump exactly in correspondence of the classical bifurcation point. This suggests that the interaction between different boundary modes is switched on by the transition and the resulting flow becomes rather sensitive to variations in the amplitude of the terms associated with the corresponding harmonics.

Finally, we notice that there exist a bulk phenomenon in the sensitivity factors within the region of fully developed convection, i.e., for $Ra > 3000$. This suggests that in such region the Nusselt number is equally sensitive to variations in the amplitude of different harmonics of the temperature expansion at the lower wall. This is expected since the heat transfer in the fully developed convection region is primarily determined by advection.

7. Summary

We have studied the Rayleigh–Bénard stability problem for a fluid confined within a square enclosure subject to non-uniform random perturbations in the temperature distribution at the horizontal walls. These temperature perturbations were modeled as Gaussian processes satisfying a Gaussian correlation function. We have simulated the Oberbeck–Boussinesq equations and computed many ensembles of realizations of the natural convective flow within the cavity by sampling the temperature processes at the boundaries for different correlation length and amplitude. This allowed us to obtain stochastic bifurcation diagrams for the integrated Nusselt number near the classical onset of convective instability. These diagrams show that random perturbations render the bifurcation process to convection imperfect, in agreement with known theoretical results [15]. In particular, the pure conduction state does no longer exist, being replaced by a quasi-conduction regime. We have observed subcritical and *nearly supercritical* quasi-conduction stable states within the range of Rayleigh numbers $Ra = 0 - 4000$. This suggests that random temperature perturbations at the horizontal walls can extend the range of stability of quasi-conduction states beyond the classical bifurcation point. However, the probability that these states develop within the cavity is rather low. A statistical analysis of the bifurcation diagrams near the classical onset of convection shows the existence of a stochastic drift phenomenon in the heat transfer coefficient, especially in the transcritical region. The increment we have observed in the mean Nusselt number is about 10% for temperature perturbations having a correlation length comparable with the sidelength of the cavity. In order to obtain a better understanding of this phenomenon, we have performed a sensitivity analysis of the integrated Nusselt number based on a functional ANOVA decomposition. This allowed us to identify which harmonics in the expansion of the random temperature distributions at the horizontal walls are most effective in enhancing the heat transfer coefficient. Indeed, the sensitivity factors corresponding to the first-, second- and third-order interaction terms suggest that the harmonic with smallest wavelength is the most effective. In addition, the flow transition from quasi-conduction to fully developed convection is found to be accurately captured by the second- and the third-order interaction terms.

Acknowledgements

This work was supported by OSD-MURI grant FA9550-09-1-0613, DOE grant DE-FG02-07ER25818 and NSF grant DMS-0915077.

Appendix A. Galerkin discretization

Let us consider an expansion of random temperature and velocity fields in terms of normalized eigenfunctions $\hat{\psi}_n(x, y)$ and $\hat{\Gamma}_m(x, y)$

$$\psi(x, y; \omega) = \sum_{n=1}^{N_v} a_n(\omega) \hat{\psi}_n(x, y), \quad (39)$$

$$T^*(x, y; \omega) = \sum_{m=1}^{N_t} b_m(\omega) \hat{\Gamma}_m(x, y). \quad (40)$$

The analytical expression of $\hat{\psi}_n$ and $\hat{\Gamma}_m$ will be given in the subsequent Sections A.1 and A.2. The advantage of using the representations (39) and (40) is that they automatically satisfy all the boundary conditions as well as the continuity equation [44,18]. We remark that higher-order spectral element discretizations of the streamfunction and the temperature fields can be also considered [45–47]. A substitution of Eqs. (39) and (40) into Eqs. (15) and (16) and subsequent Galerkin projection onto $\hat{\psi}_k$ and $\hat{\Gamma}_k$, respectively, gives the following system of algebraic equations (repeated indices are summed unless otherwise stated)

$$a_n a_m \mathcal{B}_{nmk} - \text{Pr} a_n c_{nk} + \text{RaPr} (b_n \mathcal{D}_{nk} + \mathcal{N}_k) = 0, \quad (41)$$

$$-a_n b_m \mathcal{E}_{nmk} - a_n (\mathcal{F}_{nk} + \mathcal{P}_{nk}) - \Gamma_k^2 b_k + \mathcal{M}_k = 0, \quad (42)$$

where the coefficients $\mathcal{N}_k, \mathcal{M}_k$, etc., are defined as

$$\mathcal{N}_k \stackrel{\text{def}}{=} \int_0^1 \int_0^1 \left[y \left(\frac{\partial g_2}{\partial x} - \frac{\partial g_1}{\partial x} \right) + \frac{\partial g_1}{\partial x} \right] \hat{\psi}_k dx dy,$$

$$\mathcal{M}_k \stackrel{\text{def}}{=} \int_0^1 \int_0^1 \left[y \left(\frac{\partial^2 g_2}{\partial x^2} - \frac{\partial^2 g_1}{\partial x^2} \right) + \frac{\partial^2 g_1}{\partial x^2} \right] \hat{\Gamma}_k dx dy,$$

$$\mathcal{A}_{nk} \stackrel{\text{def}}{=} \int_0^1 \int_0^1 \nabla^2 \hat{\psi}_n \hat{\psi}_k dx dy, \quad c_{nk} \stackrel{\text{def}}{=} \int_0^1 \int_0^1 \nabla^4 \hat{\psi}_n \hat{\psi}_k dx dy,$$

$$\mathcal{D}_{nk} \stackrel{\text{def}}{=} \int_0^1 \int_0^1 \frac{\partial \hat{\Gamma}_n}{\partial x} \hat{\psi}_k dx dy, \quad \mathcal{F}_{nk} \stackrel{\text{def}}{=} \int_0^1 \int_0^1 \frac{\partial \hat{\psi}_n}{\partial x} \hat{\Gamma}_k dx dy,$$

$$\mathcal{P}_{nk} \stackrel{\text{def}}{=} \int_0^1 \int_0^1 \left[\frac{\partial \hat{\psi}_n}{\partial y} \left(y \left(\frac{\partial g_2}{\partial x} - \frac{\partial g_1}{\partial x} \right) + \frac{\partial g_1}{\partial x} \right) - \frac{\partial \hat{\psi}_n}{\partial x} (g_2 - g_1) \right] \hat{\Gamma}_k dx dy,$$

$$\mathcal{B}_{nmk} \stackrel{\text{def}}{=} \int_0^1 \int_0^1 \left(\frac{\partial \hat{\psi}_n}{\partial y} \frac{\partial \nabla^2 \hat{\psi}_m}{\partial x} - \frac{\partial \hat{\psi}_n}{\partial x} \frac{\partial \nabla^2 \hat{\psi}_m}{\partial y} \right) \hat{\psi}_k dx dy,$$

$$\mathcal{E}_{nmk} \stackrel{\text{def}}{=} \int_0^1 \int_0^1 \left(\frac{\partial \hat{\psi}_n}{\partial y} \frac{\partial \hat{\Gamma}_m}{\partial x} - \frac{\partial \hat{\psi}_n}{\partial x} \frac{\partial \hat{\Gamma}_m}{\partial y} \right) \hat{\Gamma}_k dx dy.$$

Also, Γ_k^2 denote the eigenvalues of the Helmholtz equation (see Appendix A.1). The numerical solution to the nonlinear algebraic system (41) and (42) is computed through the Newton method, for a resolution of 20 basis function along each direction x and y , i.e., $N_v = 400, N_t = 400$ basis functions in the series expansions (39) and (40). The initial guesses for the streamfunction and the temperature fields in the Newton iteration are set to be random. In this way, for each specific realization of the boundary conditions, we obtain the Fourier coefficients $a_n(\omega)$ and $b_m(\omega)$. Once these coefficients are available, the streamfunction and the temperature fields can be easily recovered from Eqs. (39), (40) and (11).

A.1. Temperature expansion

We consider an eigenfunction expansion based on the classical Helmholtz equation in Cartesian coordinates

$$\nabla^2 T^* + \Gamma^2 T^* = 0, \quad (43)$$

with homogeneous boundary conditions

$$T^*(x, 0) = T^*(x, 1) = \frac{\partial T^*(0, y)}{\partial x} = \frac{\partial T^*(1, y)}{\partial x} = 0. \tag{44}$$

A separation of variables in Eq. (43) gives the following two Sturm–Liouville problems

$$\frac{d^2 X}{dx^2} + a^2 X = 0, \quad \frac{dX(0)}{dx} = \frac{dX(1)}{dx} = 0, \tag{45}$$

$$\frac{d^2 Y}{dy^2} + b^2 Y = 0, \quad Y(0) = Y(1) = 0, \tag{46}$$

whose solutions are the well known [24,25] normalized eigenfunctions

$$X_n(x) = \begin{cases} 1 & \text{if } n = 0 \\ \sqrt{2} \cos(n\pi x) & \text{if } n = 1, 2, 3, \dots \end{cases} \tag{47}$$

$$Y_m(y) = \sqrt{2} \sin(m\pi y) \quad m = 1, 2, 3, \dots, \tag{48}$$

while the eigenvalues are

$$a_n = \pi n \quad \text{for } n = 0, 1, 2, \dots, \tag{49}$$

$$b_m = \pi m \quad \text{for } m = 1, 2, \dots \tag{50}$$

This implies that the eigenvalues of (43) are

$$\Gamma_{nm}^2 = \pi^2(n^2 + m^2). \tag{51}$$

Thus, the two-dimensional temperature basis function can be written as

$$\widehat{T}_n(x, y) = X_{i(n)}(x)Y_{j(n)}(y), \tag{52}$$

where $i(n)$ and $j(n)$ are suitable subsequences obtained according an ordering of Γ_{ij}^2 .

A.2. Velocity expansion

All the velocity boundary conditions are of no-slip type. This means $\partial\psi/\partial x = \partial\psi/\partial y = 0$ everywhere at the boundary. In order to generate a divergence free basis for the velocity representation satisfying such boundary conditions it is convenient to consider the following eigenvalue problem [44,48,18,12]

$$\frac{\partial^4 \psi}{\partial x^4} + \frac{\partial^4 \psi}{\partial y^4} = A^4 \psi, \tag{53}$$

$$\psi(x, 0) = \frac{\partial\psi(x, 0)}{\partial x} = 0, \quad \psi(x, 1) = \frac{\partial\psi(x, 1)}{\partial x} = 0, \tag{54}$$

$$\psi(0, y) = \frac{\partial\psi(0, y)}{\partial y} = 0, \quad \psi(1, y) = \frac{\partial\psi(1, y)}{\partial y} = 0. \tag{55}$$

This eigenvalue problem is symmetric⁶ and separable. A substitution of the ansatz

$$\psi(x, y) = X(x)Y(y), \tag{56}$$

into (53) yields two equivalent eigenvalue problems for $X(x)$ and $Y(y)$ in the form

$$\frac{d^4 X}{dx^4} = \alpha^4 X, \tag{57}$$

$$X(0) = X(1) = \frac{\partial X(0)}{\partial x} = \frac{\partial X(1)}{\partial x} = 0. \tag{58}$$

The general integral of (57) is easily found⁷ as

$$X(x) = a \sin(\alpha x) + b \cos(\alpha x) + c \sinh(\alpha x) + d \cosh(\alpha x).$$

⁶ The spectral theory for linear operators in a Hilbert space guarantees that the eigenfunction set is then complete (the nullspace of the operator $\partial^4/\partial x^4 + \partial^4/\partial y^4$ with boundary conditions (54) and (55) is empty).

⁷ It is sufficient to consider a solution in the form $X(x) = e^{\beta x}$ to obtain, by substitution, $\beta^4 = \alpha^4$, i.e., $\beta = \{\alpha, -\alpha, i\alpha, -i\alpha\}$.

By enforcing the boundary conditions (58) we obtain the following normalized set of eigenfunctions

$$X_i(x) = \begin{cases} \cos[\alpha_i(x - 1/2)]/\cos[\alpha_i/2] - \cosh[\alpha_i(x - 1/2)]/\cosh[\alpha_i/2] & i = 1, 3, 5, \dots \\ \sin[\alpha_i(x - 1/2)]/\sin[\alpha_i/2] - \sinh[\alpha_i(x - 1/2)]/\sinh[\alpha_i/2] & i = 2, 4, 6, \dots \end{cases}$$

where the eigenvalues α_i are solutions of the transcendental equation

$$\tanh\left(\frac{\alpha_i}{2}\right) = \begin{cases} -\tan(\alpha_i/2) & \text{for } i = 1, 3, 5, \dots \\ \tan(\alpha_i/2) & \text{for } i = 2, 4, 6, \dots \end{cases} \tag{59}$$

A similar solution can be obtained for $Y(y)$. A normalized basis for the two-dimensional streamfunction can be obtained as a tensor product of one-dimensional bases as

$$\widehat{\psi}_n(x, y) = X_{i(n)}(x)Y_{j(n)}(y), \tag{60}$$

where $i(n)$ and $j(n)$ are suitable subsequences obtained according to an eigenvalue ordering

$$A_n^4 = \alpha_{i(n)}^4 + \beta_{j(n)}^4. \tag{61}$$

Appendix B. ANOVA decomposition for sensitivity analysis

The key idea of ANOVA is to represent a high-dimensional function $f(x_1, x_2, \dots, x_N)$ in terms of a superimposition of functions involving a lower number of variables (interaction terms), and then truncate the series at specific interaction order. Specifically, the ANOVA expansion of an N -dimensional scalar function f takes the form [49]

$$f(x_1, x_2, \dots, x_N) = f_0 + \sum_{i=1}^N f_i(x_i) + \sum_{i<j}^N f_{ij}(x_i, x_j) + \sum_{i<j<k}^N f_{ijk}(x_i, x_j, x_k) + \dots \tag{62}$$

The function f_0 is a constant. The functions $f_i(x_i)$, which we shall call first-order interactions, give us the overall effects of the variables x_i in f as if they were acting independently of the other input variables. The functions $f_{ij}(x_i, x_j)$ describe the interaction effects of the variables x_i and x_j , and therefore they will be called second-order interactions. Similarly, higher-order terms reflect the cooperative effects of an increasing number of variables. From a practical viewpoint, the computation of the various terms in the ANOVA expansion can be performed by selecting a suitable measure space, e.g., the space of μ -integrable functions in the hypercube $[0, 1]^N$, where μ denotes an integration measure. In this case we have

$$f_0 = \int_0^1 \dots \int_0^1 f(x_1, \dots, x_N) d\mu(x_1, \dots, x_N), \tag{63}$$

$$f_i(x_i) = \int_0^1 \dots \int_0^1 f(x_1, \dots, x_{i-1}, x_{i+1}, \dots, x_N) \times d\mu(x_1, \dots, x_{i-1}, x_{i+1}, \dots, x_N) - f_0, \tag{64}$$

For instance, if the measure μ is selected as

$$d\mu(x_1, \dots, x_N) = \prod_{i=1}^N dx_i, \tag{65}$$

then we obtain the classical ANOVA-HDMR method [23]. Similarly, if we set

$$d\mu(x_1, \dots, x_N) = \prod_{i=1}^N \delta(x_i - c_i) dx_i, \quad c_i \in [0, 1], \quad (66)$$

then we obtain the so-called *anchored* ANOVA [50] decomposition. The vector (c_1, \dots, c_N) in this case is known as *anchor point* and it can be selected according to many different criteria (see, e.g., [21]). The ANOVA representation of a field can be effectively used as a tool for sensitivity analysis [43,51]. To this end, let us first recall that all the interaction terms (63) and (64), etc., in the ANOVA expansion (62) are mutually orthogonal with respect to the measure μ . This implies that the variance of f , here denoted as $\sigma^2[f]$, is simply the sum of the variances associated with each interaction term, i.e.,

$$\sigma^2[f] = \sum_{i=1}^N \sigma^2[f_i] + \sum_{i<j}^N \sigma^2[f_{ij}] + \dots, \quad (67)$$

where

$$\sigma^2[f] \stackrel{\text{def}}{=} \int f^2 d\mu - \left(\int f d\mu \right)^2. \quad (68)$$

The integrals appearing in Eq. (67) can be computed by using a multi-element quadrature formula [33]. Following Sobol [43], we shall define the global sensitivity indices of the system as the ratio between the variance of each term in the ANOVA decomposition and the total variance of the function f , i.e.,

$$R_i \stackrel{\text{def}}{=} \frac{\sigma^2[f_i]}{\sigma^2[f]}, \quad R_{ij} \stackrel{\text{def}}{=} \frac{\sigma^2[f_{ij}]}{\sigma^2[f]}, \dots \quad (69)$$

From Eq. (67) it easily follows that

$$\sum_{i=1}^N R_i + \sum_{i<j}^N R_{ij} + \dots = 1. \quad (70)$$

Moreover, we shall define the following averaged global sensitivity indices

$$Z_i^{(1)} \stackrel{\text{def}}{=} R_i, \quad Z_i^{(2)} \stackrel{\text{def}}{=} \sum_j R_{ij}, \quad Z_i^{(3)} \stackrel{\text{def}}{=} \sum_{j,k} R_{ijk}, \dots \quad (71)$$

representing the relative importance of one specific parameter over all the others at a prescribed interaction level. With the aid of Eq. (71) we can study which input variable has more influence on the response of the system. For instance, we can quantify which harmonic in the Fourier series representation of the random temperature boundary conditions triggers the transition from quasi-conduction to convection or affects the heat transfer coefficient to the greatest extent.

References

- [1] S. Chandrasekhar, Hydrodynamic and Hydromagnetic Stability, Dover, 1981.
- [2] P.G. Drazin, W.H. Reid, Hydrodynamic Stability, Cambridge Univ. Press, 1961.
- [3] L.A. Segel, Distant side-walls cause slow amplitude modulation of cellular convection, J. Fluid Mech. 38 (1) (1969) 203–224.
- [4] P. Hall, I.C. Walton, The smooth transition to a convective regime in a two-dimensional box, Proc. R. Soc. London A 358 (1978) 199–221.
- [5] Y.A. Gelfgat, Different modes of Rayleigh–Bénard instability in two and three dimensional rectangular enclosures, J. Comput. Phys. 156 (1999) 300–324.
- [6] D. Venturi, X. Wan, G.E. Karniadakis, Stochastic bifurcation analysis of Rayleigh–Bénard convection, J. Fluid Mech. 650 (2010) 391–413.
- [7] P.G. Daniels, The effect of distant sidewalls on the transition to finite amplitude Bénard convection, Proc. R. Soc. London A 358 (1978) 173–197.
- [8] R.E. Kelly, D. Pal, Thermal convection with spatially periodic boundary conditions: resonant wavelength excitation, J. Fluid Mech. 86 (3) (1978) 433–456.
- [9] Y.A. Gelfgat, P.Z. Bar-Yoseph, Multiple solutions and stability of confined convective and swirling flows – a continuing challenge, Int. J. Numer. Meth. Heat and Fluid Flow 14 (2) (2004) 213–241.
- [10] Y.A. Gelfgat, P.Z. Bar-Yoseph, A.L. Yarin, Stability of multiple steady states of convection in laterally heated cavities, J. Fluid Mech. 338 (1999) 315–334.
- [11] D. Puigjaner, J. Herrero, C. Simó, F. Giralt, Bifurcation analysis of steady Rayleigh–Bénard convection in a cubical cavity with conducting sidewalls, J. Fluid Mech. 598 (2008) 393–427.
- [12] D. Puigjaner, J. Herrero, F. Giralt, C. Simó, Stability analysis of the flow in a cubical cavity heated from below, Phys. Fluids 16 (10) (2004) 3639–3654.
- [13] G. Freund, W. Pesch, W. Zimmermann, Rayleigh–Bénard convection in the presence of spatial temperature modulations, J. Fluid Mech. 673 (2011) 318–348.
- [14] J.M. Luijckx, J.K. Platten, On the onset of free convection in a rectangular channel, J. Non Equilib. Thermodynam. 6 (1981) 141.
- [15] G. Ahlers, C.W. Meyer, D.S. Cannell, Deterministic and stochastic effects near the convective onset, J. Stat. Phys. 54 (5/6) (1989) 1121–1131.
- [16] A. Dubi, Monte Carlo Applications in Systems Engineering, John Wiley & Sons, 2000.
- [17] K. Binder, D.W. Heermann, Monte-Carlo Simulation in Statistical Physics: and Introduction, Springer-Verlag, 1998.
- [18] M.A. Leal, H.A. Machado, R.M. Cotta, Integral transform solutions of transient natural convection in enclosures with variable fluid properties, Int. J. Heat Mass Transfer 43 (2000) 3977–3990.
- [19] L.S.D. Alves, R.M. Cotta, J. Pontes, Stability analysis of natural convection in porous cavities through integral transforms, Int. J. Heat Mass Transfer 45 (2002) 1185–1195.
- [20] Y. Cao, Z. Chen, M. Gunzburger, ANOVA expansions and efficient sampling methods for parameter dependent nonlinear PDEs, Int. J. Numer. Anal. Model. 6 (2009) 256–273.
- [21] Z. Gao, J.S. Hesthaven, On ANOVA expansions and strategies for choosing the anchor point, Appl. Math. Comput. 217 (7) (2010) 3274–3285.
- [22] X. Yang, M. Choi, G.E. Karniadakis, Adaptive ANOVA decomposition of stochastic incompressible and compressible fluid flows, J. Comput. Phys. 231 (2012) 1587–1614.
- [23] H. Rabitz, Ö.F. Aliş, J. Shorter, K. Shim, Efficient input–output model representations, Comput. Phys. Commun. 117 (1–2) (1999) 11–20.
- [24] M.N. Özisik, Heat Transfer: A Basic Approach, McGraw-Hill, 1985.
- [25] M.N. Özisik, Heat Conduction, second ed., Wiley-Interscience, 1999.
- [26] A. Papoulis, Probability, Random Variables, and Stochastic Processes, McGraw-Hill, 1991.
- [27] O. Chapelle, J. Weston, B. Schölkopf, Cluster Kernels for Semi-Supervised Learning, vol. 15, MIT Press, 2003.
- [28] A.J. Smola, R. Kondor, Kernels and regularization on graphs, in: Learning Theory and Kernel Machines: 16th Annual Conference on Learning Theory, Springer, 2003, pp. 144–172.
- [29] D. Venturi, X. Wan, G.E. Karniadakis, Stochastic low-dimensional modelling of a random laminar wake past a circular cylinder, J. Fluid Mech. 606 (2008) 339–367.
- [30] A. Segall, T. Kailath, Orthogonal functionals of independent-increment processes, IEEE Trans. Inf. Theory 22 (3) (1976) 287–298.
- [31] G. Li, S.-W. Wang, H. Rabitz, S. Wang, P. Jaffé, Global uncertainty assessments by high dimensional model representations (HDMR), Chem. Eng. Sci. 57 (21) (2002) 4445–4460.
- [32] X. Ma, N. Zabarar, An adaptive hierarchical sparse grid collocation method for the solution of stochastic differential equations, J. Comput. Phys. 228 (2009) 3084–3113.
- [33] J. Foo, G.E. Karniadakis, Multi-element probabilistic collocation method in high dimensions, J. Comput. Phys. 229 (2010) 1536–1557.
- [34] A. Nouy, Proper generalized decompositions and separated representations for the numerical solution of high dimensional stochastic problems, Arch. Comput. Methods Appl. Mech. Eng. 17 (2010) 403434.
- [35] D. Venturi, A fully symmetric nonlinear biorthogonal decomposition theory for random fields, Physica D 240 (4–5) (2010) 415–425.
- [36] D. Venturi, On proper orthogonal decomposition of randomly perturbed fields with applications to flow past a cylinder and natural convection over a horizontal plate, J. Fluid Mech. 559 (2006) 215–254.
- [37] F. Chinesta, A. Ammar, E. Cueto, Recent advances and new challenges in the use of the proper generalized decomposition for solving multidimensional models, Arch. Comput. Methods Appl. Mech. Eng. 17 (4) (2010) 327–350.
- [38] D. Venturi, T.P. Sapsis, H. Cho, G.E. Karniadakis, A computable evolution equation for the joint response–excitation probability density function of stochastic dynamical systems, Proc. R. Soc. A 468 (2139) (2012) 759–783.
- [39] A. Dhooge, W. Govaerts, Y.A. Kuznetsov, MATCONT: a matlab package for numerical bifurcation analysis of ODEs, ACM Trans. Math. Softw. 29 (2003) 141–164.
- [40] E.L. Allgower, K. Georg, Numerical Continuation Methods: An Introduction, Springer Verlag, 1990.
- [41] A.B. Owen, The dimension distribution and quadrature test functions, Statist. Sin. 13 (2003) 1–17.
- [42] X. Wang, I.H. Sloan, Why are high-dimensional finance problems often of low effective dimension?, SIAM J. Sci. Comput. 27 (2005) 159–183.
- [43] I.M. Sobol, Global sensitivity indices for nonlinear mathematical models and their Monte Carlo estimates, Math. Comput. Simul. 55 (2001) 271–280.
- [44] R.M. Cotta, Integral Transforms in Computational Heat and Fluid Flow, CRC press, Boca Raton, FL, 1993.
- [45] G.E. Karniadakis, Numerical simulation of forced convection heat transfer from a cylinder in crossflow, Int. J. Heat Mass Transfer 31 (1988) 107–118.
- [46] N.K. Ghaddar, A.T.P.G.E. Karniadakis, A conservative isoparametric spectral element method for forced convection: application to fully developed flow in periodic geometries, Numer. Heat Transfer 9 (1986) 277–300.

- [47] G.E. Karniadakis, S. Sherwin, *Spectral/hp Element Methods for Computational Fluid Dynamics*, second ed., Oxford Univ. Press, 2005.
- [48] E. Figueira, R.M. Cotta, Benchmark results for internal forced convection through integral transformation, *Int. Commun. Heat Mass Transfer* 23 (7) (1996) 1019–1029.
- [49] M. Griebel, Sparse grids and related approximation schemes for higher dimensional problems, in: L.M. Pardo, A. Pinkus, E. Süli, M.J. Todd (Eds.), *Foundations of Computational Mathematics*, Santander 2005, vol. 331, Cambridge University Press, 2006, pp. 106–161.
- [50] Z. Zhang, M. Choi, G.E. Karniadakis, Anchor points matter in ANOVA decomposition, in: J.S. Hesthaven, E.M. Rønquist (Eds.), *Spectral and High Order Methods for Partial Differential Equations*, vol. 76, Springer, 2011, pp. 347–355.
- [51] A. Saltelli, K. Chan, M. Scott, *Sensitivity Analysis*, John Wiley, 2000.